Forward-backward multiplicity fluctuations in ultrarelativistic nuclear collisions with wounded quarks and fluctuating strings

Martin Rohrmoser[1,*] and Wojciech Broniowski[1,2,†]
[1]*Institute of Physics, Jan Kochanowski University, 25-406 Kielce, Poland*
[2]*H. Niewodniczański Institute of Nuclear Physics PAN, 31-342 Cracow, Poland*

(Received 26 September 2018; published 8 February 2019)

We analyze a generic model where wounded quarks are amended with strings in which both endpoint positions fluctuate in spatial rapidity. With the assumption that the strings emit particles independently of one another and with a uniform distribution in rapidity, we are able to analyze the model semianalytically, which allows for its detailed understanding. Using as a constraint the one-body string emission functions obtained from the experimental data for collisions at $\sqrt{s_{NN}} = 200$ GeV, we explore the two-body correlations for various scenarios of string fluctuations. We find that the popular measures used to quantify the longitudinal fluctuations (a_{nm} coefficients) are limited with upper and lower bounds. These measures can be significantly larger in the model where both endpoints are allowed to fluctuate, compared to the model with single endpoint fluctuations.

DOI: 10.1103/PhysRevC.99.024904

I. INTRODUCTION

The purpose of this paper is to present a detailed semianalytic analysis of models of ultrarelativistic nuclear collisions where the early production of particles occurs from strings. The strings are associated with wounded quarks, and both of their endpoint positions fluctuate in spatial rapidity. The model generalizes the analysis of [1] where only one-end fluctuations were considered. The main assumptions are that the strings emit particles independently of one another and that the production from a string is uniform between its endpoints. We obtain the one-body string emission function from a fit to the experimental data at $\sqrt{s_{NN}} = 200$ GeV, and use it to constrain the freedom in the distribution of the endpoint positions. We then explore in detail the two-body correlations in various scenarios for the fluctuating endpoints. The derived analytic formulas allow for a full understanding of this simple model. In particular, we show that standard measures applied in analyses of the longitudinal fluctuations, such as the Legendre a_{nm} coefficients, fall between certain bounds. This explains why *a priori* different models may provide quite similar results for these measures of the longitudinal correlations. We find that the a_{nm} coefficients can be significantly larger (by a factor of $\sim$3) when one allows for two endpoints to fluctuate, compared to the case of single endpoint fluctuations of [1]. This observation is relevant for phenomenological studies. Since the model, despite its simplifications, is generic, sharing features with more complicated string implementations, our findings shed light on correlations from other string models in application to ultrarelativistic heavy-ion collisions.

The basic phenomenon explored in this paper and illustrated with definite calculations can be understood in very simple terms. Consider a string with left and right endpoints and an acceptance window in pseudorapidity. If the left endpoint were always left of the acceptance window, and the right endpoint to the right (they may fluctuate or not, but cannot enter the window), then the string seen in the window is always the same, hence no fluctuations occur. If, however, an endpoint via fluctuation enters the acceptance window, then fluctuations occur, as its observed fragment may be shorter or longer. The fluctuation effect is larger when both endpoints fluctuate into the acceptance window, which is the case explored in detail below.

The concept of wounded sources formed in the initial stages of ultrarelativistic heavy-ion collisions has proven to be phenomenologically successful in reproducing multiplicity distributions from soft particle production. The idea (see [2] for a discussion of the foundations), adopts the Glauber model [3] in its variant suitable for inelastic collisions [4]. Whereas the wounded nucleon scaling [5], when applied to the highest BNL Relativistic Heavy-Ion Collider (RHIC) or the CERN Large Hadron Collider (LHC) energies, requires a sizable admixture of binary collisions [6,7], the scaling based on wounded quarks [8–11] works remarkably well [12–28]. Another successful approach [29,30] amends the wounded nucleons with a meson-cloud component.

For mid-rapidity production, the wounded quark scaling takes the simple form

$$N_{\rm ch} = k(\langle N_A\rangle + \langle N_B\rangle), \tag{1}$$

where $N_{\rm ch}$ is the number of charged hadrons in a mid-rapidity bin, and $\langle N_i\rangle$ are the average numbers of wounded quarks in nucleus i in a considered centrality class. The proportionality constant k should not depend on centrality or the mass numbers of the nuclei (i.e., on the overall number of participants), and indeed this requirement is satisfied to expected accuracy [22,28]. Of course, k increases with the collision energy.

*mrohrmoser@ujk.edu.pl
†wojciech.broniowski@ifj.edu.pl

When it comes to modeling the rapidity spectra, formula (1) is replaced with

$$\frac{dN}{d\eta} = \langle N_A \rangle f(\eta) + \langle N_B \rangle f(-\eta), \tag{2}$$

where $f(\eta)$ is a universal (at a given collision energy) profile for emission from a wounded quark (we adopt the convention that nucleus A moves to the right and B to the left). For symmetric ($A = B$) collisions one only gets access to the symmetric part of $f(\eta)$, as then $\langle N_A \rangle = \langle N_B \rangle$. However, from asymmetric collisions, such as d-Au, one can also extract the antisymmetric component in the wounded nucleon [31] or wounded quark model [32,33] (for A-A collisions analogous analyses were carried out in [34–36]), with the finding that $f(\eta)$ is peaked in the forward region, thus quite naturally emission is in the forward direction. However, $f(\eta)$ is widely spread in the whole kinematically available range. The phenomenological result of the approximate triangular shape of the emission profile was later used in modeling the initial conditions for further evolution; see, e.g., [37–41].

Microscopically, the approximate triangular shape of the emission function finds a natural origin in color string models, where one endpoint of the string is fixed, whereas the location of the other endpoint fluctuates. In particular, in the basic Brodsky-Gunion-Kuhn mechanism [42], the emission proceeds from strings in which one endpoint is associated with a valence parton, and the other endpoint, corresponding to wee partons, is randomly generated along the space-time rapidity η. When the distribution of the fluctuating endpoint is uniform in η, and so is the string fragmentation distribution, then the triangular shape for the emission function follows.

Various Monte Carlo codes implementing the Lund string formation and decays (see, e.g., [43–48]) or the dual-parton-model/Regge-exchange approach [49–51] also introduce strings of fluctuating ends, with various specific mechanisms and effects (baryon stopping, nuclear shadowing) additionally incorporated. Apart from reproducing the measured one-body spectra, achieved by appropriate tune-ups of parameters, the incorporated initial-state correlations show up in event-by-event fluctuations that can be accessed experimentally. Thus the fluctuating strings are standard objects used in modeling the early phase of high-energy reactions.

Our model joins the concept of wounded sources with strings in the following way:

(1) Each wounded source has an associated string.
(2) The strings emit particles independently of each-other.
(3) The endpoints of a string are generated universally (in the same manner for all wounded objects) from appropriate distributions.
(4) The emission of particles from a string occurring between the endpoints is homogeneous in spatial rapidity.

In such a model, event-by-event fluctuations take the origin from fluctuations of the number of wounded objects, as well as from fluctuations of the positions of the endpoints [1]. The goal of this paper is to study this generic model, with the focus on the endpoint behavior which probes the underlying physics. We take a general approach, with no prejudice as to how the endpoints are fluctuating, but using the one-body emission profiles obtained from experiment as a physical constraint.

More complicated mechanisms associated with dense systems, such as the formation of color ropes [52,53] or nuclear shadowing, are not incorporated in our picture. Also, we consider one type of strings, which allows for simple analytic derivations.

We remark that associating a string with a leading quark is in the spirit of the Lund approach (cf. discussion of Sec. 5 in [43]). So for simplicity we have in each event N_i "wounded strings" associated with valence quarks in nucleus i. Other more complicated choices (e.g, including the binary collisions) are also possible here, but the advantage of our prescription is that by definition it complies with the experimental scaling of multiplicities of Eq. (1).

A specific implementation of some ideas explored in this work, with strings that have one end fixed and the other fluctuating, has been presented in [1].

The outline of our paper is as follows: In Sec. II we use the rapidity spectra from d-Au and Au-Au reactions at $\sqrt{s_{NN}} = 200$ GeV to obtain the one-body emission profile of the wounded quark. In Sec. III we explore our generic string model and derive simple relations between string endpoint distributions and n-body-emission profiles for the radiation from individual strings. Section IV discusses how a given one-body-emission profile can correspond to a family of different functions for the string endpoint distributions. Two-body correlations from a single string are discussed in Sec. V, whereas in Sec. VI they are combined to form the two-body correlations in nuclear collisions. Section VII presents the Legendre a_{nm} coefficients of the two-particle correlations. Finally, Sec. VIII draws the final conclusions from our work. Some more technical developments can be found in the Appendices.

II. EMISSION PROFILES FROM WOUNDED QUARKS

We begin by obtaining from experimental data the emission profiles of Eq. (2), needed in the following sections. We use the method of [31], which has also been applied recently to wounded quarks in [32]. With

$$f_s(\eta) = \tfrac{1}{2}[f(\eta) + f(-\eta)], \quad f_a(\eta) = \tfrac{1}{2}[f(\eta) - f(-\eta)], x$$
$$N_+ = N_A + N_B, \quad N_- = N_A - N_B, \tag{3}$$

one gets immediately

$$f_s(\eta) = \frac{dN/d\eta(\eta) + dN/d\eta(-\eta)}{\langle N_+ \rangle},$$
$$f_a(\eta) = \frac{dN/d\eta(\eta) - dN/d\eta(-\eta)}{\langle N_- \rangle}. \tag{4}$$

For asymmetric collisions both parts of the profile can be obtained, whereas for symmetric collisions one can only get $f_s(\eta)$.

If the wounded-quark scaling works, then the profiles obtained with different centrality classes or mass numbers of the colliding nuclei should be universal, depending only on the collision energy. To what extent this is the case can be assessed from Figs. 1 and 2, which show the one-particle

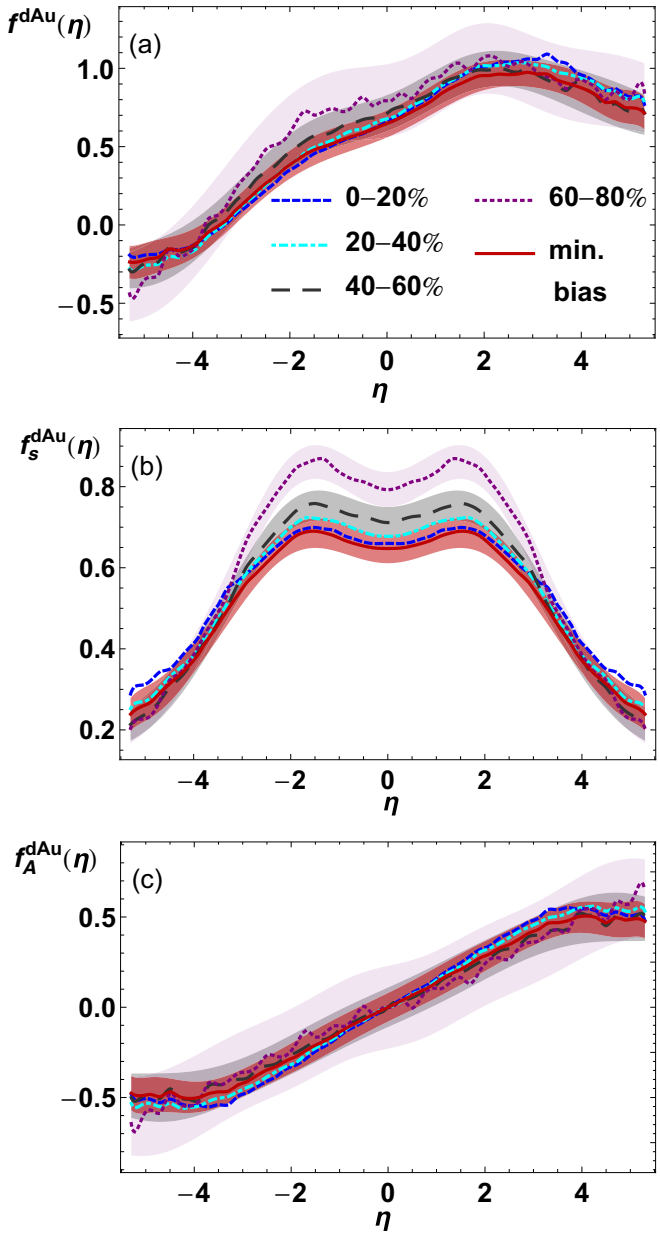

FIG. 1. One-particle emission profiles obtained in the wounded quark model via Eqs. (2)–(4) from the PHOBOS rapidity spectra for d-Au collisions at $\sqrt{s_{NN}} = 200$ GeV [54] in the indicated centrality classes (a), together with the corresponding symmetric (b) and antisymmetric (c) components. The shaded bands show the experimental uncertainties (propagated via the Gaussian method) for the 40–60% and 60–80% centrality classes, as well as for the PHOBOS minimum bias data [55].

emission profiles that were extracted from experimental data on d-Au and Au-Au collisions from the PHOBOS data [54–56] in the framework of the wounded quark model. To this end, the symmetric (for both reactions) and antisymmetric components (only in the case of the d-Au collisions) were obtained from the experimental data on rapidity spectra by means of Eq. (4), where the valence quark multiplicities $\langle N_\pm \rangle$ were obtained from GLISSANDO [57,58], a Monte Carlo simulator of the Glauber model.

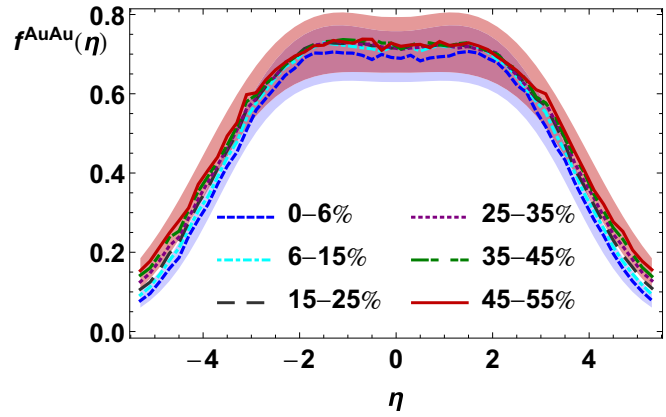

FIG. 2. One-particle emission profiles obtained in the wounded quark model from the PHOBOS rapidity spectra for Au-Au collisions at $\sqrt{s_{NN}} = 200$ GeV [56] in the indicated centrality classes. The shaded bands give the experimental uncertainties (propagated via the Gaussian method) for the most central and the most peripheral case.

Figure 1 shows the results for the one-particle emission profiles $f^{dAu}(\eta)$ extracted from the PHOBOS data [54,55] for d-Au collisions, together with their symmetric and antisymmetric components. In general, the curves for various centrality classes, considering the propagated experimental errors, can be viewed as coinciding. The apparent exception to this behavior is seen in the symmetric part of the profile for the peripheral centrality 60%–80%, which is significantly larger for $|\eta| < 3$, cf. Fig. 1(b). We note that for d-Au collisions this peripheral class corresponds to $\langle N_+ \rangle$ in the range from six to eight sources, which are tiny values, where the model admittedly does not work. It can thus confirm the findings of [32] that the assumption of universality of the one-particle emission profiles works reasonably well for the central to mid-peripheral d-Au collisions, whereas it starts to differ for more peripheral centrality classes.

Figure 2 presents our results for the one-particle emission profiles $f^{AuAu}(\eta)$ extracted from the PHOBOS data [56] for Au-Au collisions. As already mentioned, in this case only the symmetric parts of the emission profiles can be obtained. It can be seen that the results for $f^{AuAu}(\eta)$ in various centrality classes agree remarkably well with one another. They also approximately agree with the symmetric profiles for d-Au collisions of Fig. 1(b).

Finally, we test if our method reproduces the PHOBOS charged particle rapidity spectra for combined d-Au and Au-Au collisions. To this end we take a single "universal" $f(\eta)$, consisting of an antisymmetric part extracted from the minimum-bias d-Au spectra and a symmetric part taken as the average of the different one-particle emission profiles of Au-Au collisions shown in Fig. 2. The charged particle rapidity spectra $dN_{\rm ch}/d\eta$ were calculated by means of Eq. (2) with this universal $f(\eta)$, where again the numbers $\langle N_A \rangle$ and $\langle N_B \rangle$ were generated with GLISSANDO. Figure 3 shows the resulting one-particle emission spectra for d-Au and Au-Au collisions obtained that way, together with the corresponding experimental data from PHOBOS [54–56]: As expected from Fig. 2, the rapidity spectra for the Au-Au collisions, which

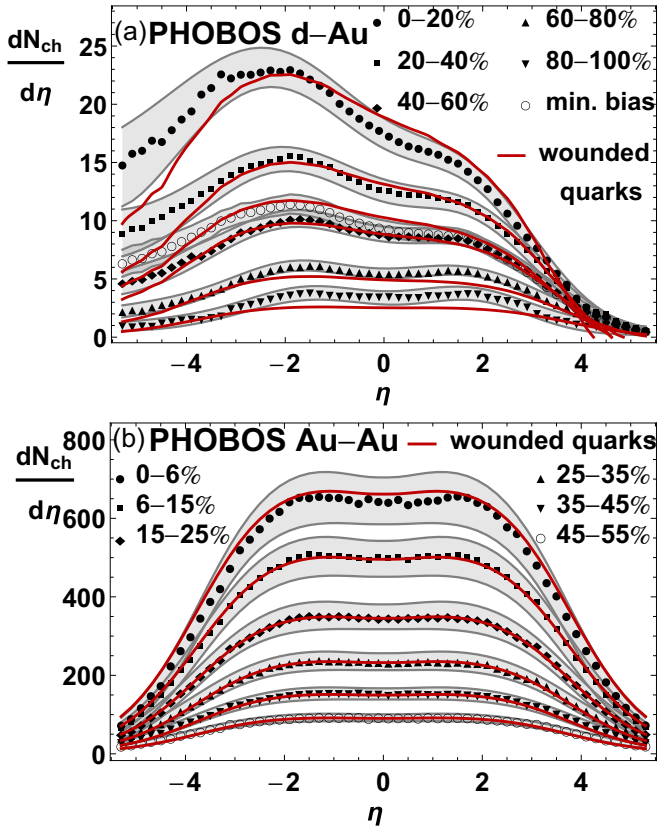

FIG. 3. Comparison of the wounded-quark model predictions (lines) with the experimental rapidity spectra (points) for d-Au [54] (a) and Au-Au [56] (b) collisions, with the experimental uncertainties shown as shaded bands. A universal profile discussed in the text is taken for the model calculations in all cases.

are almost symmetric, are very well reproduced by the chosen $f(\eta)$. Also the rapidity spectra for the d-Au collisions, which largely depend on both the symmetric and antisymmetric contribution to $f(\eta)$, are qualitatively well reproduced for $|\eta| < 4$, except for the above-discussed case of the peripheral collisions.

Therefore, we conclude that the wounded quark model with the universal profile function $f(\eta)$ reproduces the experimental rapidity spectra at $\sqrt{s_{NN}} = 200$ GeV in a way satisfactory for our exploratory study.[1] In the following analysis of the rapidity fluctuations, we use the $f(\eta)$ obtained here to constrain the string endpoint distributions.

III. GENERIC STRING MODEL

In this section we describe a model of generic production from a single string formed in the early phase of the collision process. Suppose the string is pulled by two endpoints placed at spatial rapidities y_1 and y_2, whose locations are generated according to a probability distribution $g(y_1, y_2)$ [if the endpoints are generated in an uncorrelated manner, then $g(y_1, y_2) = g_1(y_1)g_2(y_2)$, as will be assumed shortly]. The emission of a particle with rapidity η from the string fragmentation process is assumed to be uniformly distributed along the string, i.e., it is equal to

$$s(\eta; y_1, y_2) = \omega[\theta(y_1 < \eta < y_2) + \theta(y_2 < \eta < y_1)], \quad (5)$$

where ω is a dimensionless constant determining the production strength and $\theta(c)$ imposes the condition c. Note that we include the cases of $y_2 > y_1$ and $y_1 > y_2$, which may seem redundant but which is needed, for instance, when the two endpoints correspond to different partons in a given model.

Let us introduce the shorthand notation

$$\int_{\mathcal{Y}} dy_1\, dy_2\, g(y_1, y_2) X = \langle X \rangle_{\mathcal{Y}}, \quad (6)$$

with $\mathcal{Y}$ denoting the two-dimensional range of integration, depending on the kinematic constraints and/or detector coverage, and X meaning any expression. The single-particle density for production from a string upon averaging over the fluctuation of the endpoints is therefore

$$f(\eta) = \langle s(\eta; y_1, y_2) \rangle_{\mathcal{Y}}, \quad (7)$$

Analogously, for the n-particle production ($n \geqslant 2$) from a single string we have

$$f_n(\eta_1, \ldots, \eta_n) = \langle s(\eta_1; y_1, y_2) \cdots s(\eta_n; y_1, y_2) \rangle_{\mathcal{Y}}, \quad (8)$$

where we have assumed independent production of the n particles.

In case the string ends are generated independently of each other, one has

$$\langle X \rangle_{\mathcal{Y}} = \int dy_1 dy_2\, g_1(y_1) g_2(y_2) X, \quad (9)$$

where the limits of integration in y_i are formally from $-\infty$ to ∞, with the support taken care of by the forms of $g_i(y_i)$. Then we readily find that the one-body emission profile is

$$\begin{aligned} f(\eta) &= \omega\{G_1(\eta)[1 - G_2(\eta)] + G_2(\eta)[1 - G_1(\eta)]\} \\ &= \omega\left\{\tfrac{1}{2} - 2\left[G_1(\eta) - \tfrac{1}{2}\right]\left[G_2(\eta) - \tfrac{1}{2}v\right]\right\}, \end{aligned} \quad (10)$$

where the appropriate cumulative distribution functions (CDFs) are defined as

$$G_i(y) = \int_{-\infty}^{y} dy' g_i(y'). \quad (11)$$

The profile $f(\eta)$ acquires a specific value at the arguments η_1 and η_2 where the CDFs reach $\frac{1}{2}$, i.e.,

$$\eta_1^{(0)}: \quad G_1\left(\eta_1^{(0)}\right) = \tfrac{1}{2}, \quad \eta_2^{(0)}: \quad G_2\left(\eta_2^{(0)}\right) = \tfrac{1}{2}. \quad (12)$$

Then from Eq. (10) we obtain

$$\omega = 2f\left(\eta_1^{(0)}\right) = 2f\left(\eta_2^{(0)}\right). \quad (13)$$

This equation provides a special meaning to the constant ω. Furthermore, since $0 \leqslant G_{1,2}(\eta) \leqslant 1$, Eq. (10) yields the limit

$$0 \leqslant f(\eta) \leqslant \omega. \quad (14)$$

The above features will be explored shortly in a qualitative discussion.

[1] We note that the analogous analysis at the LHC leads to somewhat less accurate agreement, which calls for improvement of the model.

Similarly, for the n-particle distributions with $n \geqslant 2$ we have

$$f_n(\eta_1, \ldots, \eta_n) = \omega^n \{G_1(\min(\eta_1, \ldots, \eta_n))[1 - G_2(\max(\eta_1, \ldots, \eta_n))] + G_2(\min(\eta_1, \ldots, \eta_n))[1 - G_1(\max(\eta_1, \ldots, \eta_n))]\}. \quad (15)$$

We thus see that in the model with two endpoints fluctuating [the relevant assumptions are the uniform string fragmentation (5) and the independence of the two endpoint locations] all the information carried by the n-particle densities produced from a single string is encoded solely in the cumulative distributions functions G_1 and G_2. It is obvious, however, that G_1 and G_2 cannot be separately determined from the one-body distributions in an unambiguous manner, hence a large degree of freedom is still left in the model after fixing the rapidity spectra. Yet, the one body distribution provides, via Eq. (10), an important constraint. Our method of matching G_1 and G_2 to the one-body function $f(\eta)$ is explained in detail in Appendix A. As we stress, there is no uniqueness in the procedure, but there is a systematic way of approaching the problem, allowing one to explore the range of possibilities.

We denote the position of the maximum of $f(\eta)$ as $\eta_{\max}$. We consider three cases:

(i) The distributions of both endpoints are equal, $g_1(\eta) = g_2(\eta)$, Eq. (A3). In this case $\omega = 2f(\eta_{\max})$, with $\eta_{\max} = \eta_1^{(0)} = \eta_2^{(0)}$.
(ii) The supports of distributions $g_1(\eta)$ and $g_2(\eta)$ do not overlap, Eq. (A4). In this case $\omega = f(\eta_{\max})$ and $\eta_2^{(0)} < \eta_{\max} < \eta_1^{(0)}$.
(iii) The form of $g_1(\eta)$ is motivated by parton distribution functions (PDFs) of valence quarks, Eq. (B6), and $g_2(\eta)$ is adjusted according to Eq. (A5).

Cases (i) and (ii) are in a sense most different, showing the span of possibilities formally allowed, whereas case (iii) is intermediate. For case (iii) we use the parametrization of the valence quark PDF given by Eq. (B6) with parameters $\alpha = -0.5$ and $\beta = 3$, which are typical values at low scales. We have found that using other reasonable parametrizations has very small influence on our results, with case (iii) always remaining close to case (i).

We stress that all the considered cases reproduce, by construction, the one-body emission profiles $f(\eta)$.

We end this section with remarks concerning the model with one end of the string fixed and the other one fluctuating, explored in [1]. This simplified version can be obtained as a special limit from Eqs. (10) and (15) by choosing $g_1(\eta) = \delta(\eta - y_{\max})$, which is equivalent of taking, correspondingly, $G_1 = 0$ for $\eta < y_{\max}$, i.e.,

$$f(\eta) = \omega G_2(\eta),$$
$$f_n(\eta_1, \ldots, \eta_n) = \omega^n G_2(\min(\eta_1, \ldots, \eta_n)). \quad (16)$$

We note immediately that this model cannot reproduce $f(\eta)$ for $\eta > \eta_{\max}$, as $G_2(\eta)$ cannot decrease. Thus the model is limited to $\eta \leqslant \eta_{\max}$, which, however, is not a problem if we are only interested in the mid-rapidity region.

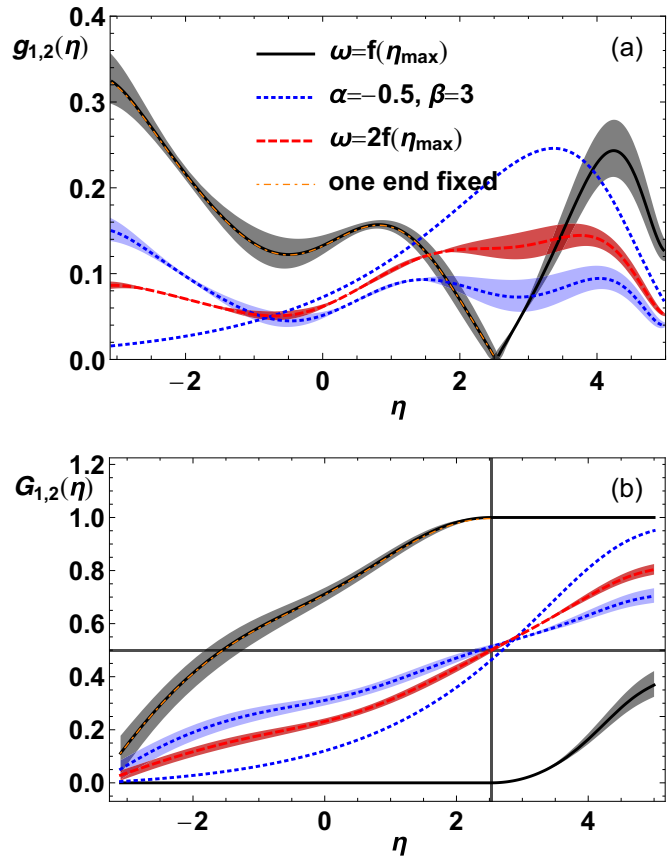

FIG. 4. Distribution functions g_1 and g_2 (a) and cumulative distribution functions G_1 and G_2 (b) of the string endpoints for the cases of (i) $\omega = 2f(\eta_{\max})$, (ii) $\omega = f(\eta_{\max})$, and (iii) $\alpha = -0.5$, $\beta = 3$, as indicated in the legend. The light dot-dashed line corresponds to the model with one endpoint fixed and the other one fluctuating [1], which overlaps with case (ii) for $\eta \leqslant \eta_{\max}$. The vertical line in panel (b) indicates $\eta = \eta_{\max}$. See the text for further details.

Moreover, in this region the single-end fluctuating model corresponds precisely to case (ii) of the two-end fluctuations. This is obvious from the following argumentation: When the right end of the string is fluctuating outside of the acceptance region, it is irrelevant if it fluctuates or if it is fixed, as in both cases we only observe the production from the part of the string falling into the acceptance range. In that situation (or more precisely for $\eta \leqslant \eta_{\max}$) Eqs. (10) and (15) reduce to Eqs. (16). Hence, the single endpoint fluctuation model of [1] corresponds to the present case (ii) at $\eta \leqslant \eta_{\max}$, and is not applicable for $\eta > \eta_{\max}$.

IV. ENDPOINT DISTRIBUTIONS

We now come to the discussion of the endpoint distributions subjected to the requirement that the one-body emission profiles are reproduced.

Figure 4(a) shows the distributions of the string endpoints, g_1 and g_2, for the three cases, and Fig. 4(b) the corresponding CDFs, G_1 and G_2. The shaded bands give an estimate of the errors due to the experimental uncertainty Δf for the one-particle emission profile f. In the case of Fig. 4(b), the

upper limit of the shaded bands corresponds to the values of $G_{1,2}$ that are matched to the one-body profile $f + \Delta f$, whereas the lower limits are matched to $f - \Delta f$. For these upper and lower limits of $G_{1,2}$, the derivatives in η yield the upper and lower limits of the shaded bands for g_1 and g_2 depicted in Fig. 4(a). For case (iii) a shaded band is given only for g_2 (G_2). This is because by construction g_1 (G_1) coming from PDFs are assumed to be accurate and all uncertainty is therefore attributed to g_2 (G_2).

In case (i) $g_1(\eta) = g_2(\eta)$, hence the distributions are indicated with a single curve (solid line) in Figs. 4(a) and 4(b). We note that the distribution of $g_1(\eta)$ peaks at forward rapidity (the Au side), as expected from the shape of the one-body profile $f(\eta)$ in Fig. 1. The CDF crosses the value $1/2$ at $\eta_1^{(0)} = \eta_2^{(0)} = \eta_{\max} \simeq 2.5$, which coincides with the maximum of $f(\eta)$.

In case (ii) (dashed lines in Fig. 4) the supports for g_1 and g_2 are disjoint. In Fig. 4(a) the left part of the curve, up to the point $\eta_{\max} \simeq 2.5$ (indicated with a vertical line), corresponds to g_2, and the right part to g_1. Hence, the string endpoints always follow the ordering $y_1 \geqslant y_2$, which does not hold in the other cases. Figure 4(b) shows the corresponding CDFs, with $G_1 = 0$ left from $\eta_{\max}$, and $G_2 = 1$ right from $\eta_{\max}$. In Appendix A we show that G_1 and G_2 from case (ii) are the lower and upper limits for any CDFs in the considered problem. Indeed, the CDFs from the other two cases fall in between these limiting curves.

Case (iii), based on a valence quark PDF for g_1, represents an intermediate class of distributions falling between cases (i) and (ii). The curves corresponding to the valence quark are dotted and with no error bands. The distribution g_1 (valence quark) is peaked in the forward direction, as expected. We note that $y_1 > y_2$ is favored, although $y_2 < y_1$ is also possible. With the parametrization we used of the valence quark distribution, the CDFs in case (iii) are not far from case (i). We have checked that this feature holds also for other reasonable parametrizations of the valence quark PDF.

We underline again that all the cases of Fig. 4, which exhibit radically different endpoint distributions, reproduce by construction the one-body emission profile $f(\eta)$.

V. CORRELATIONS FROM A SINGLE STRING

As we show in this section, the two-particle correlation is sensitive to the particular form of the distributions and differs between cases (i), (ii), and (iii). A convenient quantity is the covariance of the two-particle emission from a single string, defined as

$$\mathrm{cov}(\eta_1, \eta_2) = f_2(\eta_1, \eta_2) - f(\eta_1) f(\eta_2), \tag{17}$$

where f_2 is given by Eq. (15). Explicitly,

$$\begin{aligned}\mathrm{cov}(\eta_1, \eta_2) = \omega^2 \{ & G_1(\min(\eta_1, \eta_2))[1 - G_2(\max(\eta_1, \eta_2))] \\ & + G_2(\min(\eta_1, \eta_2))[1 - G_1(\max(\eta_1, \eta_2))] \\ & - (G_1(\eta_1)[1 - G_2(\eta_1)] + G_2(\eta_1)[1 - G_1(\eta_1)]) \\ & \times (G_1(\eta_2)[1 - G_2(\eta_2)] + G_2(\eta_2)[1 - G_1(\eta_2)])\}.\end{aligned} \tag{18}$$

A simplification occurs along the diagonal $\eta_1 = \eta_2 = \eta$, where

$$\begin{aligned}\mathrm{cov}(\eta, \eta) &= \omega^2 \left\{ \tfrac{1}{4} - 4 \left[G_1(\eta) - \tfrac{1}{2} \right]^2 \left[G_2(\eta) - \tfrac{1}{2} \right]^2 \right\} \\ &= f(\eta)[\omega - f(\eta)].\end{aligned} \tag{19}$$

Also, the leading expansion at the diagonal in the antidiagonal direction, with $\eta_1 = \eta + \delta$ and $\eta_2 = \eta - \delta$, yields a very simple formula,

$$\begin{aligned}&\mathrm{cov}(\eta + \delta, \eta - \delta) \\ &\quad = \mathrm{cov}(\eta, \eta) - \omega^2 [g_1(\eta) + g_2(\eta)] |\delta| + O(\delta^2).\end{aligned} \tag{20}$$

Figure 5 shows the resulting distributions for $\mathrm{cov}(\eta_1, \eta_2)$ for the three considered cases. One observes vivid qualitative differences between the covariances in cases (i) and (ii); cf. Figs. 5(a) and 5(b). Whereas in case (i) the covariance exhibits a monotonously increasing ridge along the $\eta_1 = \eta_2$ direction, the covariance in case (ii) shows a double peak structure, with a zero at $\eta = \eta_{\max} \simeq 2.5$, which corresponds to the zero of g_1 and g_2 in Fig. 4(a). At this point $G_1(\eta) = 0$ and $G_2(\eta) = 1$, which upon substitution to Eq. (18) yields zero. Another difference is in magnitude of the covariance, which in case (i) is significantly larger than in case (ii).

The covariance in case (iii) is very close to case (i) [cf. Figs. 5(a) and 5(c)]. Some small difference can be seen where η_1 is small (large), but η_2 large (small), where in case (iii) the covariance noticeably drops to negative values.

We also note that in all cases the values on the diagonal is obeying Eq. (19). The fall-off from the diagonal in the antidiagonal direction is given by the second term in Eq. (20). We note that the slope is proportional to $4 f(\eta_{1,2}^{(0)})[g_1(\eta) + g_2(\eta)]$, hence two models which have similar values of $\eta_{1,2}^{(0)}$ and close sums of the two endpoint distributions, $g_1(\eta) + g_2(\eta)$, will have similar covariances in the vicinity of the diagonal. Both conditions are satisfied between models (i) and (iii). In particular, we can see that the sum $g_1(\eta) + g_2(\eta)$ for model (iii) in Fig. 4(a) (dotted lines) is close to twice $g_{1,2}(\eta)$ for model (i) (solid line).

Thus the reason for the similarity of correlations in cases (i) and (iii) may be traced back to Eq. (20), which shows that this is the average of $g_1(\eta)$ and $g_2(\eta)$, which controls the fall-off of the correlation from the diagonal. These averages happen to be very similar when we use any reasonable parametrization of the parton distribution function giving the PDF of one endpoint distribution, and the fluctuations the other endpoint are adjusted to match the profile function $f(\eta)$, as explained in Sec. IV.

VI. CORRELATIONS FROM MULTIPLE STRINGS

As already discussed in the Introduction, in our approach the strings "belong" to the valence quarks either from nucleus A or from nucleus B. With the underlying assumptions of independent wounded sources, the expressions for the n-body distributions account for the combinatorics in a simple manner, with the particles at rapidities η_i being products from a string belonging to A or to B. For the one-body density in A-B

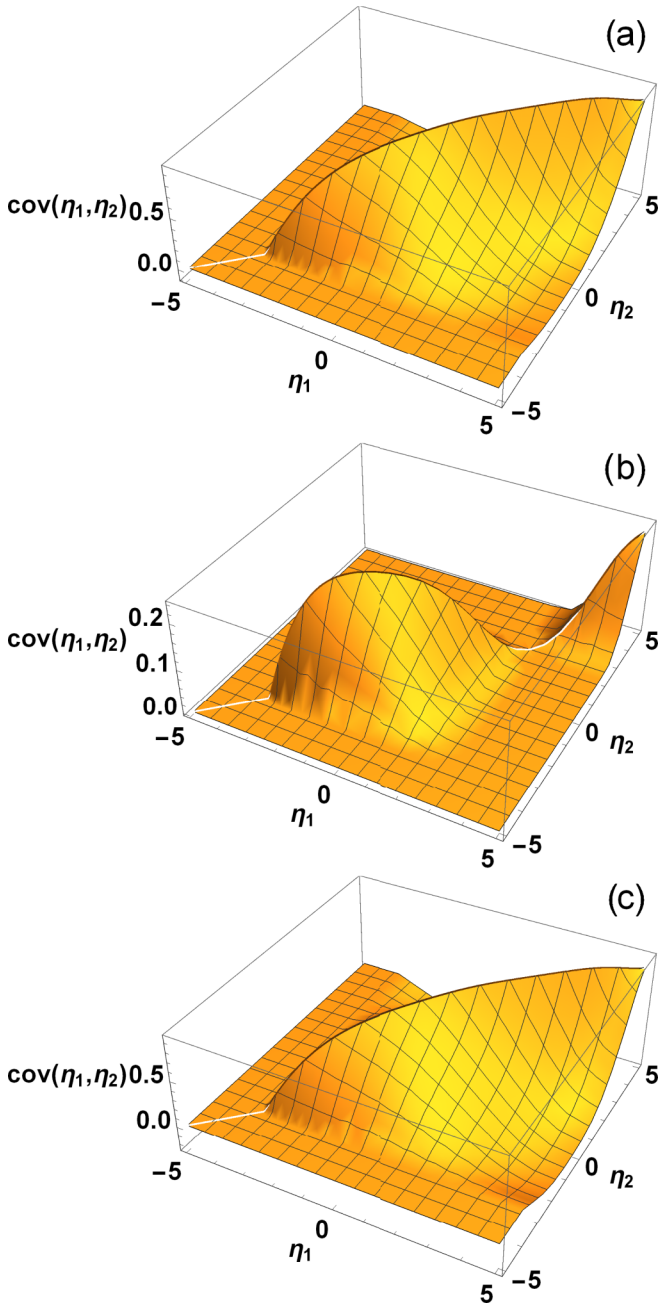

FIG. 5. Covariance for the emission from a single string for cases (i) (a), (ii) (b), and (iii) (c).

collisions one finds

$$f_{AB}(\eta) = \langle N_A\rangle f_A(\eta) + \langle N_B\rangle f_B(\eta), \tag{21}$$

where $\langle N_A\rangle$ and $\langle N_B\rangle$ are the event-by-event average numbers of wounded sources in nuclei A and B, respectively, and $f_{A,B}(\eta) = f(\pm\eta)$ denote the profiles for the emission from a single string, as given by Eq. (7), associated with sources from nuclei A or B. We work in the nucleon-nucleon center-of-mass (CM) frame, hence $f_A(\eta) = f_B(-\eta)$.

Analogously, one can define the two-body distribution for emission from a single string in nuclei A and B as $f_{A,B}(\eta_1,\eta_2) = f_2(\pm\eta_1,\pm\eta_2)$, and the corresponding covariances as $\mathrm{cov}_{A,B}(\eta_1,\eta_2) = \mathrm{cov}(\pm\eta_1,\pm\eta_2)$. Then, one readily obtains the covariance for the production in A-B collisions (see Appendix C) in the form

$$\begin{aligned}\mathrm{cov}_{AB}(\eta_1,\eta_2) &\equiv f_{AB}(\eta_1,\eta_2) - f_{AB}(\eta_1)f_{AB}(\eta_2)\\ &= \langle N_A\rangle \mathrm{cov}_A(\eta_1,\eta_2) + \langle N_B\rangle \mathrm{cov}_B(\eta_1,\eta_2)\\ &\quad + \mathrm{var}(N_A) f_A(\eta_1) f_A(\eta_2) + \mathrm{var}(N_B) f_B(\eta_1)\\ &\quad \times f_B(\eta_2) + \mathrm{cov}(N_A,N_B)[f_A(\eta_1)f_B(\eta_2)\\ &\quad + f_B(\eta_1)f_A(\eta_2)].\end{aligned} \tag{22}$$

In the special case of symmetric collisions, Eq. (22) simplifies into

$$\begin{aligned}\mathrm{cov}_{AB}(\eta_1,\eta_2) &= \langle N_A\rangle \mathrm{cov}_A(\eta_1,\eta_2) + \langle N_B\rangle \mathrm{cov}_B(\eta_1,\eta_2)\\ &\quad + \mathrm{var}(N_+) f_s(\eta_1) f_s(\eta_2) + \mathrm{var}(N_-) f_a(\eta_1)\\ &\quad \times f_a(\eta_2),\end{aligned} \tag{23}$$

where $N_- = N_A - N_B$. The moments of N_A and N_B evaluated with GLISSANDO are listed in Appendix D.

We also introduce the customary correlation C defined as

$$C_{AB}(\eta_1,\eta_2) = 1 + \frac{\mathrm{cov}_{AB}(\eta_1,\eta_2)}{f_{AB}(\eta_1)f_{AB}(\eta_2)}, \tag{24}$$

which is a convenient measure due to its intensive property. For symmetric collisions Eq. (24) becomes

$$C_{AB}(\eta_1,\eta_2) = 1 + \frac{\mathrm{cov}_{AB}(\eta_1,\eta_2)}{\langle N_+\rangle^2 f_s(\eta_1)f_s(\eta_2)}, \tag{25}$$

To separate the contribution from the string endpoint fluctuations, we also define

$$C^*_{AB}(\eta_1,\eta_2) = \frac{\langle N_A\rangle \mathrm{cov}_A(\eta_1,\eta_2) + \langle N_B\rangle \mathrm{cov}_B(\eta_1,\eta_2)}{f_{AB}(\eta_1)f_{AB}(\eta_2)}. \tag{26}$$

We note that Eq. (22) or (23) contain terms with two classes of fluctuations: those stemming from single string endpoint fluctuations, containing $\mathrm{cov}_i(\eta_1,\eta_2)$, which were the object of study in the previous section, and the remaining terms [59] with moments of fluctuations of the numbers of wounded quarks, N_A and N_B. Therefore the correlation function $C(\eta_1,\eta_2)$ contains a mixture of both effects. In principle, one could separate these effects via the technique of partial covariance (see, e.g., [60,61]), which effectively imposes constraints on a multivariate sample. The details of such an analysis, which leads to very simple and practical expressions, were presented in [62].

In the present case, however, such an analysis is not necessary if we have in mind the standard a_{nm} coefficients discussed in Sec. VII. As is clear from Eq. (25), the term $\mathrm{var}(N_+)f_s(\eta_1)f_s(\eta_2)$ in Eq. (23) brings in a constant $\mathrm{var}(N_+)/\langle N_+\rangle^2$ into $C(\eta_1,\eta_2)$. Therefore it only changes its baseline and does not affect the a_{nm} coefficients (for $n,m \geqslant 0$). As we shall shortly see, the string endpoint fluctuations given by the term with $\langle N_A\rangle \mathrm{cov}_A(\eta_1,\eta_2) + \langle N_B\rangle \mathrm{cov}_B(\eta_1,\eta_2)$ are largely dominant over the Bzdak-Teaney [59] term, $\mathrm{var}(N_-)f_a(\eta_1)f_a(\eta_2)$, with the later entering at a level of 10–20% in a_{11} (cf. Sec. VII). Hence one may simply take the view that measuring the a_{nm} coefficients associated with $C(\eta_1,\eta_2)$

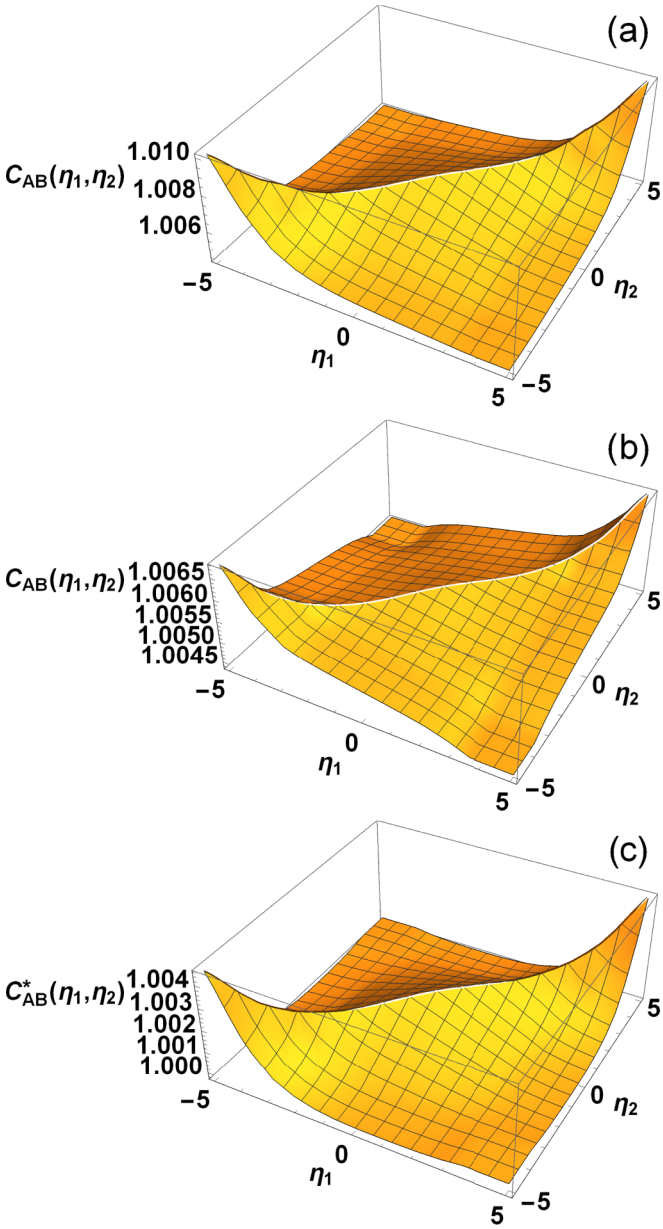

FIG. 6. Correlations $C_{AB}(\eta_1, \eta_2)$ for the 6% most central Au-Au collisions for model cases (i) (a) and (ii) (b), as well as $C^*_{AB}(\eta_1, \eta_2)$ for case (i) (c).

essentially provides information on the string endpoint fluctuations, with only a small contamination by the fluctuation of the number of sources.

Panels (a) and (b) of Fig. 6 show our results for $C_{AB}(\eta_1, \eta_2)$ of the 6% most central Au-Au collisions at $\sqrt{s_{NN}} = 200$ GeV in cases (i) and (ii) of our model. The correlations exhibit a ridge structure along the $\eta_1 = \eta_2$ direction, which simply reflects the presence of the ridges in the single-string fluctuations displayed in Fig. 5. The correlation in case (iii) is very close to case (i), simply reflecting the behavior of Fig. 5, hence we do not include it in the plot.

Panel (c) shows the correlation stemming from the fluctuation of the string endpoint, $C^*_{AB}(\eta_1, \eta_2)$ of Eq. (26). We note that, apart for an overall shift by a constant, it is very similar to the correlation $C_{AB}(\eta_1, \eta_2)$ of Eq. (24), which indicates an important feature shown by our study: The shape of the correlation function $C(\eta_1, \eta_2)$ is largely dominated by the string endpoint fluctuations, whereas the effects of the fluctuations of the number of sources are small.

VII. a_{nm} COEFFICIENTS

For a given correlation function $C(\eta_1, \eta_2)$, the a_{nm} coefficients are defined as [59,63,64]

$$a_{nm} = \int_{-Y}^{Y} \frac{d\eta_1}{Y} \int_{-Y}^{Y} \frac{d\eta_2}{Y} \frac{1}{\mathcal{N}_C} C(\eta_1, \eta_2) T_n\left(\frac{\eta_1}{Y}\right) T_m\left(\frac{\eta_2}{Y}\right), \tag{27}$$

with the normalization constant

$$\mathcal{N}_C = \int_{-Y}^{Y} \frac{d\eta_1}{Y} \int_{-Y}^{Y} \frac{d\eta_2}{Y} C(\eta_1, \eta_2), \tag{28}$$

where $[-Y, Y]$ is the covered pseudorapidity range. Having in mind the typical pseudorapidity acceptance at RHIC, we use $Y = 1$. The functions $T_n(x)$ form a set of orthonormal polynomials. The choice used in [63–65] is

$$T_n(x) = \sqrt{n + 1/2} P_n(x), \tag{29}$$

where $P_n(x)$ are the Legendre polynomials.

Analogously, we define

$$a^*_{nm} = \int_{-Y}^{Y} \frac{d\eta_1}{Y} \int_{-Y}^{Y} \frac{d\eta_2}{Y} \frac{1}{\mathcal{N}_C} C^*(\eta_1, \eta_2) T_n\left(\frac{\eta_1}{Y}\right) T_m\left(\frac{\eta_2}{Y}\right), \tag{30}$$

which focuses on the fluctuations of the strings [note that the normalization constant $\mathcal{N}_C$ is evaluated with $C(\eta_1, \eta_2)$ as in Eq. (27)] .

Figure 7 shows our results for a_{11} [panel (a)] and a^*_{11} [panel (b)] obtained for Au-Au collisions at $\sqrt{s_{NN}} = 200$ GeV and plotted as functions of the average number of wounded quarks $\langle N_+ \rangle$ in selected centrality classes. We note that the results for model cases (i) and (iii) are essentially identical, reflecting the feature seen already in Fig. 6. The result for case (ii) is about a factor of 3 smaller. In this and following figures we also indicate the results for the model with single endpoint fluctuations, which is identical to case (ii) in the considered acceptance region.

In view of the discussion of Sec. IV, cases (i) and (ii) in Fig. 7 represent the upper and lower bounds for the admissible values of the a_{11} coefficients. This is an important result, as it provides the possible range for this quantity in approaches sharing the features of our model.

In panel (c) of Fig. 7 we present the ratio a^*_{11}/a_{11}, which shows the announced dominance of the string endpoint fluctuations over the fluctuation of the numbers of sources. In model cases (i) and (iii) the former account for 90% of the effects, whereas in case (ii) they account for 75–85%.

From Eqs. (23) and (26) it is clear that a^*_{11} scales as $1/\langle N_+ \rangle$. For a_{11} there is a small departure of a relative order

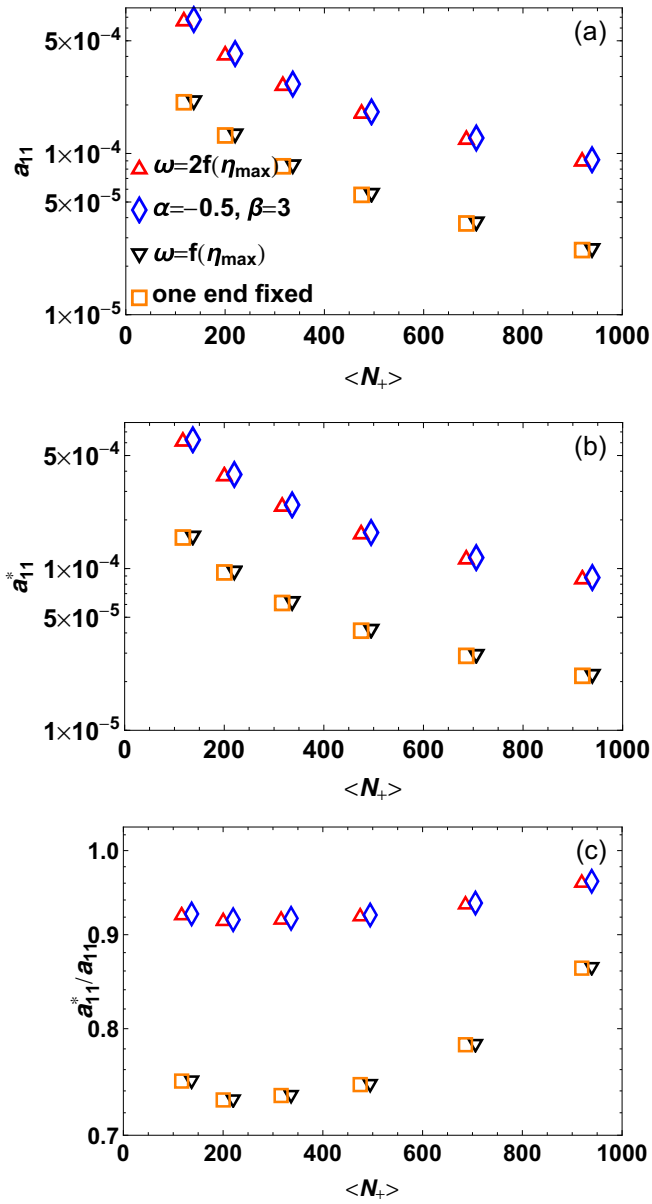

FIG. 7. a_{11} (a) and a^*_{11} (b) for Au-Au collisions at $\sqrt{s_{NN}} =$ 200 GeV as a function of $\langle N_+\rangle$ (the selected values for $\langle N_+\rangle$ correspond to the 6 centrality classes 0–6%, 6–15%, 15–25%, 25–35%, 35–45%, and 45–55%) in cases (i) with $\omega = 2f(\eta_{\max})$, (ii) with $\omega = f(\eta_{\max})$, (iii) with $\alpha = -0.5$, $\beta = 3$, together with the model of [1] with one endpoint fixed, as indicated in the legend. Panel (c) displays the ratio a^*_{11}/a_{11}. To enhance visibility, the markers for the overlapping cases are slightly shifted to the left or right along the abscissa.

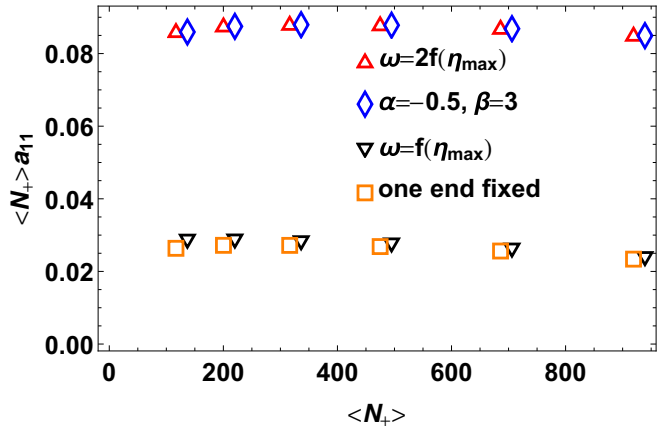

FIG. 8. The product of a_{11} and $\langle N_+\rangle$, showing the scaling discussed in the text.

var$(N_-)/\langle N_+\rangle$. Numerically, for models (i) and (ii) $a^*_{11} \sim 0.08/\langle N_+\rangle$, whereas the leading term of expansion (20) yields a close result, $a^*_{11} \sim 0.1/\langle N_+\rangle$. The approximate scaling for a_{11} is exhibited in Fig. 8.

A similar analysis of the a_{11} coefficients for the d-Au collisions yields qualitatively similar results, shown in Fig. 9. Here, the coefficients a^*_{11} account for more than 90% of the total, hence the dominance of string endpoint fluctuations is even more pronounced in d-Au than in Au-Au collisions. For that reason we present only the results for a_{11}.

In addition to a_{11} coefficients, one may study the higher-order a_{nm} coefficients. We give our results for a_{13} and a_{22} from Au-Au collisions in Fig. 10. While these coefficients are considerably suppressed as compared to a_{11}, shown in Fig. 10, they exhibit the same qualitative behavior. In particular, they scale almost exactly as $1/\langle N_+\rangle$.

Finally, we remark that when the model results are to be compared to experimental values, one needs to relate the space-time rapidity of the initial stage, $\eta_{PS} = \frac{1}{2}\ln[(t + z)/(t - z)]$ (until now denoted as η in our considerations), to the momentum pseudorapidity of the measured hadrons, $\eta = \frac{1}{2}\ln[(E + p_z)/(E - p_z)]$. The experience of hydrodynamic simulations shows a mild longitudinal push, yielding $\eta \simeq 1.25\,\eta_{PS}$. This effect leads to a quenching factor of about 1.5 to be applied to the model a_{nm} coefficients before comparing to the data.

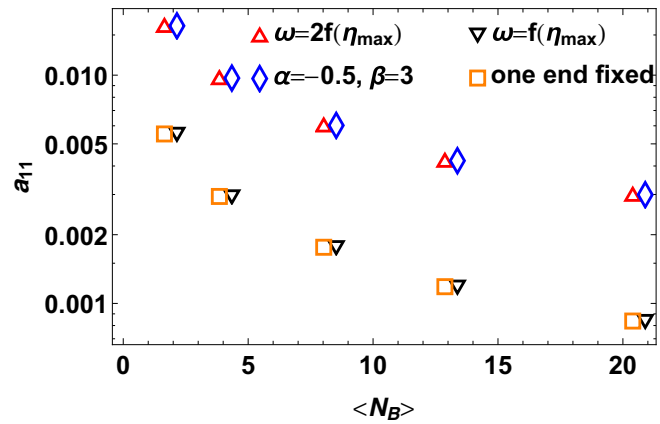

FIG. 9. Same as in Fig. 7(a) but for d-Au collisions at $\sqrt{s_{NN}} =$ 200 GeV, plotted as a function of the average number of wounded quarks in Au, $\langle N_B\rangle$ (selected values for $\langle N_B\rangle$ correspond to centrality classes 0–20%, 20–40%, 40–60%, 60–80%).

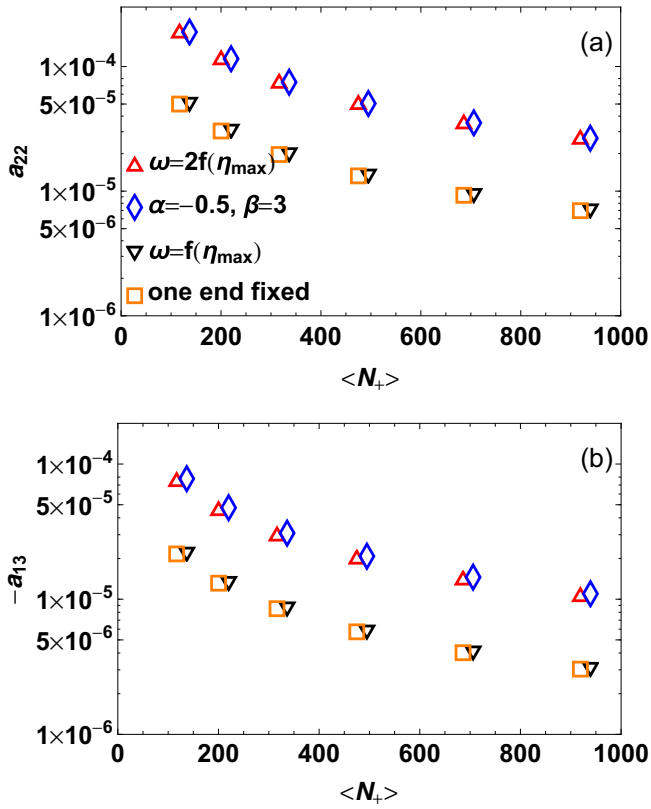

FIG. 10. Same as in Fig. 7(a) but for a_{22} (a) and $-a_{13}$ (b).

VIII. CONCLUSIONS

We have analyzed a model where strings are associated with wounded quarks and their endpoints fluctuate. We have used the data for the pseudorapidity spectra for d-Au and Au-Au collisions from the PHOBOS Collaboration at $\sqrt{s_{NN}} = 200$ GeV to impose constraints on the one-body distributions in the model. We have selected a RHIC energy for our study, since the wounded quark model works very well in this case.

We first confirmed the results of [32] that a thus-extracted one-body emission function reproduces reasonably well the experimental rapidity spectra and therefore is universal in the sense that it can be applied to different centrality classes and collision systems for the considered collision energy. Then we showed that there remains a substantial freedom in string endpoint distributions $G_{1,2}$, which gives rise to a family of possible solutions. Specifically, we have discussed three cases of solutions: the limiting cases (i) and (ii) and an intermediate case (iii), inspired by the valence quark parton distribution function. We have argued that case (ii) is equivalent to the model with single endpoint fluctuations of [1], if the acceptance window at mid-rapidity is sufficiently narrow.

The analysis was carried out analytically, which has its obvious merits. We obtained formulas for the n-body distributions of the produced particles. In the study of the two-body correlations, we have examined the effects from string endpoint fluctuations and from the fluctuation of the number of sources. The former largely dominate in the corresponding Legendre coefficients a_{nm}.

We have found that the range for fluctuations is limited by two extreme cases. The lower limit, where the domains of the fluctuations of both ends do not overlap, coincides (for sufficiently narrow acceptance windows in pseudorapidity) with the model with single-end fluctuations considered earlier in [1]. Allowing for both ends to fluctuate increases significantly the fluctuations, raising the a_{nm} coefficients by a factor of $\sim$3.

A variant of the model where the distribution of one end of the string follows the valence quark PDF, is very close to the case giving maximum correlation [our case (i)]. Our results, in particular the presented bounds, can serve as a baseline for future data analysis of the forward-backward fluctuations in rapidity at $\sqrt{s_{NN}} = 200$ GeV.

Our simple approach, while neglecting many possible effects such as mutual influence of the strings (merging into color ropes, nuclear shadowing), short range correlations of various origin, or assuming strings of only one type, incorporates two basic and generic features: fluctuation of the number of strings and fluctuation of the location of the string endpoints. This makes its predictions valuable for understanding the underlying mechanisms. It remains to be seen to what extent our analytic approach can be extended to more general models, in particular going beyond the simple Glauber wounded picture.

ACKNOWLEDGMENTS

Research supported by the Polish National Science Centre (NCN) Grant No. 2015/19/B/ST2/00937.

APPENDIX A: MATCHING THE CUMULATIVE DISTRIBUTION FUNCTIONS TO ONE-BODY EMISSION PROFILES

It is convenient to introduce the shifted CDFs

$$H_i(\eta) = G_i(\eta) - \tfrac{1}{2}, \tag{A1}$$

which grow from the value $-1/2$ up to $1/2$. Then Eq. (10) can be rewritten as

$$H_1(\eta)H_2(\eta) = \frac{1}{4} - \frac{1}{2\omega} f(\eta). \tag{A2}$$

We shall now consider three specific cases.[2] In the first case, the maximum of $f(\eta)$ is taken to be $\omega/2$, which is the lowest possible value [otherwise it would contradict Eq. (13)]. The position of the maximum is at $\eta_0 = \eta_0^{(1)} = \eta_0^{(2)}$ [the two zeros of $H_i(\eta)$ coincide in this case]. Then the solution takes the form

$$H_1(\eta) = \sqrt{\frac{1}{4} - \frac{1}{2\omega} f(\eta)}\, \mathrm{sgn}(\eta - \eta_0) s(\eta),$$
$$H_2(\eta) = \sqrt{\frac{1}{4} - \frac{1}{2\omega} f(\eta)}\, \mathrm{sgn}(\eta - \eta_0)/s(\eta), \tag{A3}$$

where sgn denotes the sign function, and $s(\eta)$ is an arbitrary function chosen in such a way that the required limiting and

[2]We assume in the derivation of the first two cases that $f(\eta)$ is unimodal, as is the case of the phenomenologically fitted profile.

monotonicity properties of $H_i(\eta)$ are preserved [one possibility, which we use, is $s(\eta) = 1$, in which case both distributions are the same].

The second special case is when the maximum of $f(\eta)$ is ω, which is the largest possible value. Then one may choose

$$H_1(\eta) = -\frac{1}{2}\theta(\eta_0 - \eta) + \left[\frac{1}{2} - \frac{1}{\omega}f(\eta)\right]\theta(\eta - \eta_0),$$
$$H_2(\eta) = -\left[\frac{1}{2} - \frac{1}{\omega}f(\eta)\right]\theta(\eta_0 - \eta) + \frac{1}{2}\theta(\eta - \eta_0). \quad \text{(A4)}$$

In this case the supports of $g_1(\eta)$ and $g_2(\eta)$ are disjoint.

We can now easily verify that the formulas (A3) and (A4) indeed satisfy Eq. (A2).

In the intermediate case, when the maximum satisfies $\omega/2 < f(\eta) \leqslant \omega$, one may generically take a "favorite" form of $H_1(\eta)$ and then evaluate $H_2(\eta)$ from Eq. (A2) as

$$H_2(\eta) = \frac{\frac{1}{4} - \frac{1}{2\omega}f(\eta)}{H_1(\eta)}. \quad \text{(A5)}$$

Note that $H_2(\eta)$ is well behaved near η_1, as in its vicinity

$$H_1(\eta) = C_1^2(\eta - \eta_1) + \cdots,$$
$$\frac{f(\eta)}{\omega} = \frac{1}{2} - C_2^2(\eta - \eta_1)^2 + \cdots, \quad \text{(A6)}$$

where C_1^2 and C_2^2 denote positive constants, hence

$$H_2(\eta) = \frac{C_2^2}{2C_1^2}(\eta - \eta_1) + \cdots. \quad \text{(A7)}$$

One needs to check explicitly if $H_2(\eta)$ obtained from Eq. (A5) is a growing function, otherwise the initial choice of $H_1(\eta)$ is inconsistent.

Since $-\frac{1}{2} \leqslant H_1(\eta) \leqslant \frac{1}{2}$, it follows immediately from Eq. (A5) that

$$H_2(\eta) \geqslant \frac{1}{2} - \frac{1}{\omega}f(\eta) \quad \text{for } \eta \geqslant \eta_0,$$
$$H_2(\eta) \leqslant -\frac{1}{2} - \frac{1}{\omega}f(\eta) \quad \text{for } \eta \leqslant \eta_0 \quad \text{(A8)}$$

(and similarly for H_1), hence the expressions (A4) provide upper and lower limits for *any* CDF for the considered problem.

APPENDIX B: PDF-MOTIVATED DISTRIBUTION

When the string endpoints $y_{1,2}$ are associated with subnucleonic constituents, such as a valence or sea quark, gluon, or diquark, then they carry the fractions x_{iA} or x_{iB} of the longitudinal momenta of the nucleons inside beams A and B, respectively. Specifically, if the momentum of the constituent is k_{iA} (k_{iB}) and the momentum of the nucleon is P_A (P_B), then from standard kinematic considerations the corresponding rapidity y_{iA} (y_{iB}) of the endpoint is related to x_{iA} (x_{iB}) with the exact formula

$$x_{iA} \equiv \frac{k_{iA}^+}{P_A^+} = \frac{m_{Ti}}{M}e^{y_{iA}-y_b},$$
$$x_{iB} \equiv \frac{k_{iB}^+}{P_B^+} = \frac{m_{Ti}}{M}e^{-y_{iB}-y_b}, \quad \text{(B1)}$$

where $m_{T\,i} = \sqrt{m_i^2 + k_{T\,i}^2}$ is the transverse mass of the constituent, M is the mass of the nucleon, and y_b is the rapidity of beam A (in the assumed CM frame of the nucleon-nucleon collision, $-y_b$ is the rapidity of beam B).

The distributions of the locations of the string endpoints are then defined via partonic distributions $p_i(x)$ as follows:

$$g_i(y_{iQ})dy_{iQ} = p_i(x_{iQ}(y_{iQ}))dx_{iQ}, \quad \text{(B2)}$$

with $Q = A, B$, or for the corresponding CDFs

$$G_i(y_{iQ}) = P_i(x_{iQ}(y_{iQ})). \quad \text{(B3)}$$

Since $x_{i\,Q} \in [0, 1]$, the limits for the rapidities of the endpoints are $y_{iA} \in (-\infty, y_{i\uparrow}]$ and $y_{iB} \in [-y_{i\uparrow}, \infty)$, where

$$y_{i\uparrow} = y_b + \ln\left(\frac{M}{m_{Ti}}\right). \quad \text{(B4)}$$

In the CM reference frame of the nucleon-nucleon collision, the rapidity of the beam is

$$y_b = \ln\frac{\sqrt{s/4} + \sqrt{s/4 - M^2}}{\sqrt{s/4} - \sqrt{s/4 - M^2}} \simeq \ln\frac{\sqrt{s}}{M}, \quad \text{(B5)}$$

therefore at $\sqrt{s} \gg M$ we have to a good approximation $y_{i\uparrow} \simeq \ln\frac{\sqrt{s}}{m_{Ti}}$.

In the example used in this paper, a simple parametrization of the parton distribution functions (PDF) is used. Following many phenomenological studies, we take

$$p(x) = Ax^\alpha(1 - x)^\beta, \quad \text{(B6)}$$

with the corresponding CDF

$$P(x) = \frac{B(x, 1 + \alpha, 1 + \beta)}{B(1, 1 + \alpha, 1 + \beta)}, \quad \text{(B7)}$$

where $B(z, a, b)$ denotes the incomplete Euler beta function.

APPENDIX C: 2-BODY DENSITY

When we consider the two-body density of particles produced from multiple strings formed in A-B collisions, there are several combinatorial cases which may occur: the two particles may originate from the same string associated with A, from different strings associated with A, from the same string associated with B, from different strings associated with B, and finally one particle is emitted from a string associated with A and the other from a string associated with B. Thus, the two-body density averaged over events in A-B collisions takes the form

$$f_{AB}(\eta_1, \eta_2)$$
$$= \langle N_A\rangle f_A(\eta_1, \eta_2) + \langle N_A(N_A - 1)\rangle f_A(\eta_1)f_A(\eta_2)$$
$$+ \langle N_B\rangle f_B(\eta_1, \eta_2) + \langle N_B(N_B - 1)\rangle f_B(\eta_1)f_B(\eta_2)$$
$$+ \langle N_AN_B\rangle[f_A(\eta_1)f_B(\eta_2) + f_B(\eta_1)f_A(\eta_2)], \quad \text{(C1)}$$

We define the covariances in the usual way,

$$\mathrm{cov}_A(\eta_1, \eta_2) = f_A(\eta_1, \eta_2) - f_A(\eta_1)f_A(\eta_2),$$
$$\mathrm{cov}_B(\eta_1, \eta_2) = f_B(\eta_1, \eta_2) - f_B(\eta_1)f_B(\eta_2). \quad \text{(C2)}$$

TABLE I. First few moments of the wounded quark numbers in Au-Au collisions at $\sqrt{s_{NN}} = 200$ GeV as obtained from GLISSANDO simulations. The chosen centrality classes correspond to those in the PHOBOS experiment.

Centrality (%)	$\langle N_+ \rangle$	var(N_+)	var(N_-)
0–6	929	4280	502
6–15	696	4649	653
15–25	484	2972	563
25–35	326	1472	399
35–45	210	811	262
45–55	126	396	144

TABLE II. Same as in Table I but for d-Au collisions at $\sqrt{s_{NN}} = 200$ GeV. Here N_A and N_B denote the number of wounded quarks in d and Au, respectively.

Centrality (%)	$\langle N_A \rangle$	$\langle N_B \rangle$	var(N_A)	var(N_B)	cov(N_A, N_B)
0–20	5.9	20.6	0.1	14.8	0.1
20–40	5.3	13.1	0.8	2.8	−0.3
40–60	4.1	8.3	1.0	2.7	−0.4
60–80	2.8	4.1	0.6	1.4	0.0
80–100	1.6	1.9	0.3	0.3	−0.1

Then

$$f_{AB}(\eta_1,\eta_2) = \langle N_A\rangle \mathrm{cov}_A(\eta_1,\eta_2) + \langle N_A^2\rangle f_A(\eta_1) f_A(\eta_2) + \langle N_B\rangle \mathrm{cov}_B(\eta_1,\eta_2) + \langle N_B^2\rangle f_B(\eta_1) f_B(\eta_2) + \langle N_A N_B\rangle [f_A(\eta_1) f_B(\eta_2) + f_B(\eta_1) f_A(\eta_2)], \quad \text{(C3)}$$

and Eq. (22) follows.

APPENDIX D: MOMENTS OF THE WOUNDED QUARK DISTRIBUTIONS

The lowest moments of the wounded quark distributions obtained form GLISSANDO [57,58] and used in our analysis are collected in Tables I and II.

[1] W. Broniowski and P. Bożek, Phys. Rev. C **93**, 064910 (2016).
[2] A. Białas, J. Phys. G **35**, 044053 (2008).
[3] R. J. Glauber, in *Lectures in Theoretical Physics*, edited by W. E. Brittin and L. G. Dunham (Interscience, New York, 1959), Vol. 1, p. 315.
[4] W. Czyż and L. C. Maximon, Ann. Phys. (NY) **52**, 59 (1969).
[5] A. Białas, M. Błeszyński, and W. Czyż, Nucl. Phys. B **111**, 461 (1976).
[6] B. B. Back *et al.* (PHOBOS Collaboration), Phys. Rev. C **65**, 031901 (2002).
[7] D. Kharzeev and M. Nardi, Phys. Lett. B **507**, 121 (2001).
[8] A. Białas, W. Czyż, and W. Furmański, Acta Phys. Pol. B **8**, 585 (1977).
[9] A. Białas, K. Fiałkowski, W. Słomiński, and M. Zieliński, Acta Phys. Pol. B **8**, 855 (1977).
[10] A. Białas and W. Czyż, Acta Phys. Pol. B **10**, 831 (1979).
[11] V. V. Anisovich, Yu. M. Shabelski, and V. M. Shekhter, Nucl. Phys. B **133**, 477 (1978).
[12] S. Eremin and S. Voloshin, Phys. Rev. C **67**, 064905 (2003).
[13] P. K. Netrakanti and B. Mohanty, Phys. Rev. C **70**, 027901 (2004).
[14] A. Białas and A. Bzdak, Phys. Lett. B **649**, 263 (2007).
[15] A. Białas and A. Bzdak, Phys. Rev. C **77**, 034908 (2008).
[16] B. Alver, M. Baker, C. Loizides, and P. Steinberg, arXiv:0805.4411.
[17] G. Agakishiev *et al.* (STAR Collaboration), Phys. Rev. C **86**, 014904 (2012).
[18] S. S. Adler *et al.* (PHENIX Collaboration), Phys. Rev. C **89**, 044905 (2014).
[19] C. Loizides, J. Nagle, and P. Steinberg, SoftwareX **1–2**, 13 (2015).
[20] A. Adare *et al.* (PHENIX Collaboration), Phys. Rev. C **93**, 024901 (2016).
[21] R. A. Lacey, P. Liu, N. Magdy, M. Csanád, B. Schweid, N. N. Ajitanand, J. Alexander, and R. Pak, Universe **4**, 22 (2018).
[22] P. Bożek, W. Broniowski, and M. Rybczyński, Phys. Rev. C **94**, 014902 (2016).
[23] L. Zheng and Z. Yin, Eur. Phys. J. A **52**, 45 (2016).
[24] E. K. G. Sarkisyan, A. N. Mishra, R. Sahoo, and A. S. Sakharov, Phys. Rev. D **94**, 011501 (2016).
[25] J. T. Mitchell, D. V. Perepelitsa, M. J. Tannenbaum, and P. W. Stankus, Phys. Rev. C **93**, 054910 (2016).
[26] O. S. K. Chaturvedi, P. K. Srivastava, A. Kumar, and B. K. Singh, Eur. Phys. J. Plus **131**, 438 (2016).
[27] C. Loizides, Phys. Rev. C **94**, 024914 (2016).
[28] M. J. Tannenbaum, Mod. Phys. Lett. A **33**, 1830001 (2017).
[29] B. G. Zakharov, JETP Lett. **104**, 6 (2016) [Pisma Zh. Eksp. Teor. Fiz. **104**, 8 (2016)].
[30] B. G. Zakharov, J. Exp. Theor. Phys. **124**, 860 (2017).
[31] A. Białas and W. Czyż, Acta Phys. Pol. B **36**, 905 (2005).
[32] M. Barej, A. Bzdak, and P. Gutowski, Phys. Rev. C **97**, 034901 (2018).
[33] A. Adare *et al.* (PHENIX Collaboration), Phys. Rev. Lett. **121**, 222301 (2018).
[34] M. Gaździcki and M. I. Gorenstein, Phys. Lett. B **640**, 155 (2006).
[35] A. Bzdak and K. Woźniak, Phys. Rev. C **81**, 034908 (2010).
[36] A. Bzdak, Phys. Rev. C **80**, 024906 (2009).
[37] A. Adil, M. Gyulassy, and T. Hirano, Phys. Rev. D **73**, 074006 (2006).
[38] P. Bożek and I. Wyskiel, Phys. Rev. C **81**, 054902 (2010).
[39] P. Bożek and W. Broniowski, Phys. Rev. C **88**, 014903 (2013).
[40] A. Monnai and B. Schenke, Phys. Lett. B **752**, 317 (2016).
[41] S. Chatterjee and P. Bożek, Phys. Rev. C **96**, 014906 (2017).
[42] S. J. Brodsky, J. F. Gunion, and J. H. Kuhn, Phys. Rev. Lett. **39**, 1120 (1977).
[43] B. Andersson, G. Gustafson, G. Ingelman, and T. Sjostrand, Phys. Rep. **97**, 31 (1983).
[44] X.-N. Wang and M. Gyulassy, Phys. Rev. D **44**, 3501 (1991).
[45] Z.-W. Lin, C. M. Ko, B.-A. Li, B. Zhang, and S. Pal, Phys. Rev. C **72**, 064901 (2005).

[46] T. Sjöstrand, S. Ask, J. R. Christiansen, R. Corke, N. Desai, P. Ilten, S. Mrenna, S. Prestel, C. O. Rasmussen, and P. Z. Skands, Comput. Phys. Commun. **191**, 159 (2015).
[47] C. Bierlich, G. Gustafson, L. Lönnblad, and H. Shah, J. High Energ. Phys. 10 (2018) 134.
[48] S. Ferreres-Solé and T. Sjöstrand, Eur. Phys. J. C **78**, 983 (2018).
[49] A. Capella, U. Sukhatme, C.-I. Tan, and J. Tran Thanh Van, Phys. Rep. **236**, 225 (1994).
[50] K. Werner, I. Karpenko, T. Pierog, M. Bleicher, and K. Mikhailov, Phys. Rev. C **82**, 044904 (2010).
[51] T. Pierog, I. Karpenko, J. M. Katzy, E. Yatsenko, and K. Werner, Phys. Rev. C **92**, 034906 (2015).
[52] T. S. Biro, H. B. Nielsen, and J. Knoll, Nucl. Phys. B **245**, 449 (1984).
[53] H. Sorge, Phys. Rev. C **52**, 3291 (1995).
[54] B. B. Back *et al.* (PHOBOS Collaboration), Phys. Rev. C **72**, 031901 (2005).
[55] B. B. Back *et al.* (PHOBOS Collaboration), Phys. Rev. Lett. **93**, 082301 (2004).
[56] B. B. Back *et al.*, Phys. Rev. Lett. **91**, 052303 (2003).
[57] W. Broniowski, M. Rybczyński, and P. Bożek, Comput. Phys. Commun. **180**, 69 (2009).
[58] M. Rybczyński, G. Stefanek, W. Broniowski, and P. Bożek, Comput. Phys. Commun. **185**, 1759 (2014).
[59] A. Bzdak and D. Teaney, Phys. Rev. C **87**, 024906 (2013).
[60] H. Cramer, *Mathematical Methods of Statistics*, Princeton Mathematical Series, No. 9. (Princeton University Press, Princeton, 1946).
[61] W. Krzanowski, *Principles of Multivariate Analysis*, Oxford Statistical Science Series (Oxford University Press, Oxford, 2000).
[62] A. Olszewski and W. Broniowski, Phys. Rev. C **96**, 054903 (2017).
[63] G. Aad *et al.* (ATLAS Collaboration), CERN Document Server, ATLAS-CONF-2015-020.
[64] G. Aad *et al.* (ATLAS Collaboration), CERN Document Server, ATLAS-CONF-2015-051.
[65] J. Jia, S. Radhakrishnan, and M. Zhou, Phys. Rev. C **93**, 044905 (2016).